Finite-Reynolds-Number Effects in Steady, Three-Dimensional Airway Reopening

Andrew L. Hazel & Matthias Heil
School of Mathematics, University of Manchester

February 2, 2006

In print in:
ASME Journal of Biomechanical Engineering

Abstract

Motivated by the physiological problem of pulmonary airway reopening, we study the steady propagation of an air finger into a buckled elastic tube, initially filled with viscous fluid. The system is modelled using geometrically non-linear, Kirchhoff–Love shell theory, coupled to the free-surface Navier–Stokes equations. The resulting three-dimensional, fluid-structure-interaction problem is solved numerically by a fully-coupled finite element method. Our study focuses on the effects of fluid inertia, which has been neglected in most previous studies. The importance of inertial forces is characterised by the ratio of the Reynolds and capillary numbers, Re/Ca, a material parameter. Fluid inertia has a significant effect on the system's behaviour, even at relatively small values of Re/Ca. In particular, compared to the case of zero Reynolds number, fluid inertia causes a significant increase in the pressure required to drive the air finger at a given speed.

1 Introduction

The pulmonary airways are elastic vessels lined by a thin liquid film. Such vessels are susceptible to a fluid-elastic instability that can lead to their collapse and occlusion by the liquid in the film, which redistributes to form a liquid bridge [1–7]. If the airways remain occluded for significant periods of time then gas exchange will be severely impaired with potentially fatal consequences. The reopening of collapsed airways is believed to occur via the propagation of an air finger into the lungs [8]. The aim of any treatment is to ensure that the propagating air finger clears the liquid blockage and reopens the airways as quickly as possible, but without damaging the lungs. Consequently, the primary aim of theoretical and experimental studies is to determine the propagation speed of the air finger, U, as a function of the applied bubble pressure, p_b^*.

The first experimental study of the problem was performed by Gaver *et al.* [8], who investigated the propagation of an air finger into a strongly-buckled, thin-walled, polyethylene tube, filled with a high-viscosity oil. The large aspect ratio of the collapsed tube's cross sections motivated the development of a two-dimensional model: a semi-infinite bubble propagating into a fluid-filled, elastic-walled channel [9]. The behaviour of the two-dimensional system was later found to be qualitatively similar to that of a three-dimensional model of steady airway reopening developed by Hazel & Heil [10].

The structure of the p_b^*–U curve was first established by Gaver *et al.* [9], who found a generic two-branch behaviour. This behaviour also occurs in the 3D model, as shown in Fig. 1. At high speeds, the physically expected behaviour is observed and an increase in bubble pressure causes an increase in propagation speed. In this regime, termed the 'peeling' branch, the tip of the bubble is close to the tube walls and appears to 'peel' them apart; see inset in Fig. 1. At low speeds, the behaviour changes and a decrease in bubble pressure is required to increase the propagation speed of the air finger. In this regime, termed the 'pushing' branch, a large volume of fluid is 'pushed' ahead of the

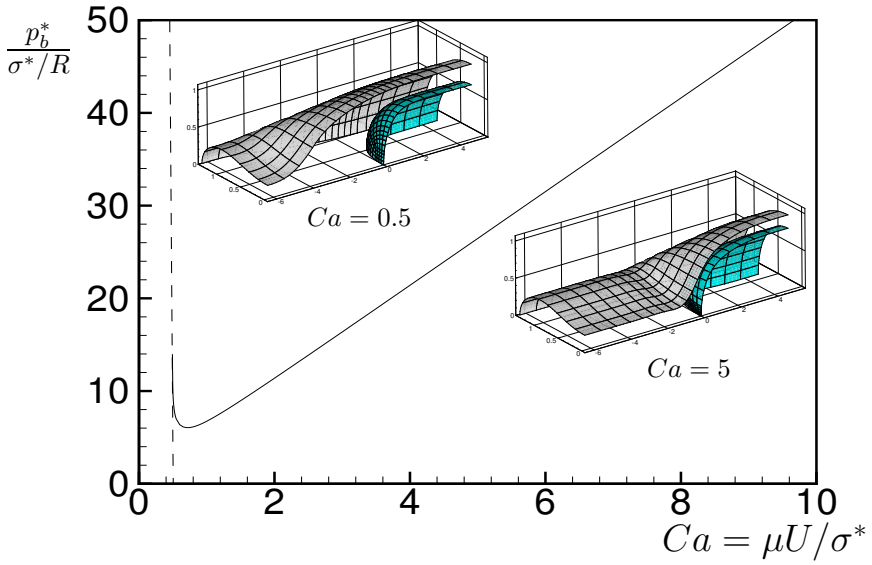

Figure 1: Bubble pressure vs. capillary number in the absence of fluid inertia (zero Reynolds number) for generic system parameters ($\nu = 0.49$, $h/R = 1/20$, $\sigma = 1$, $A_\infty = 0.373$; see §2 for parameter definitions). The dashed line is an asymptotic approximation for the behaviour on the 'pushing' branch. Inset figures illustrate tube and interface shapes on the two branches (adapted from [10]).

bubble tip, now located far from the tube walls; see second inset in Fig. 1. The 'pushing' branch is likely to be unstable if the flow is driven by a prescribed pressure; see Halpern *et al.* [11] for an analysis of this issue in the 2D model problem. For the two-dimensional model, Gaver *et al.* [9] showed that the existence of the 'pushing' branch can be deduced from conservation of mass and the fact that the film thickness behind the bubble tends to zero as the propagation speed tends to zero. Hazel & Heil [10] recognised that the same arguments also apply in three dimensions and, hence, developed an asymptotic model for the 'pushing' branch, the results of which are shown as the dashed line in Fig. 1. From a clinical point of view, the most interesting result is the prediction of a minimum pressure, $p^*_{\rm min}$, where the two branches connect and below which there are no steady solutions.

Extensions to the two-dimensional airway-reopening model have included studies of the effects of surfactant [12, 13]; the effects of wall permeability [14] and an asymptotic model of the 2D 'peeling' branch [15]. The above-mentioned studies all neglected fluid inertia, an approximation thought to be justified by the small values of the Reynolds number in the small airways. However, Heil [16] showed that in the two-dimensional problem fluid inertia can have a surprisingly large effect even at low values of the Reynolds number. It is not clear, *a priori*, that the effects of fluid inertia will be the same in the two- and three-dimensional systems, and so the aim of the present paper is to analyse the effect of fluid inertia in three-dimensional airway reopening.

2 The Model

Following Hazel & Heil [10], we model airway reopening as the steady propagation of an inviscid air finger into a buckled, elastic tube containing an incompressible, Newtonian liquid of viscosity μ, density ρ and a constant surface tension, σ^*, at the air-liquid interface. The internal pressure of the air finger is p_b^* and its propagation speed is U. The tube has an undeformed radius R, wall thickness h, Young's modulus E, Poisson's

ratio, ν and the cross-sectional area of the tube far ahead of the air finger is A^*_∞.

There are four dimensionless parameters governing the system:

$$Ca = \frac{\mu U}{\sigma^*}, \quad Re = \frac{\rho U R}{\mu}, \quad \sigma = \frac{\sigma^*}{RK} \text{ and } A_\infty = \frac{A^*_\infty}{4R^2}, \tag{1}$$

where $K = E(h/R)^3/12(1-\nu^2)$ is the bending modulus of the tube. Ca, the capillary number, is the ratio of viscous to surface-tension forces; Re, the Reynolds number, is the ratio of inertial to viscous forces; σ is the dimensionless surface tension, which represents the ratio of surface-tension forces to the tube's bending stiffness; and A_∞ is the dimensionless cross-sectional area and is a measure of the initial degree of collapse of the tube.

We formulate the problem in Cartesian coordinates, $\boldsymbol{x} = (x_1, x_2, x_3) = \boldsymbol{x}^*/R$, and choose R as the characteristic lengthscale. An asterisk is used throughout this paper to distinguish dimensional quantities from their dimensionless equivalents. U is chosen to be the fluid velocity scale, $\boldsymbol{u} = \boldsymbol{u}^*/U$ and the fluid pressure is non-dimensionalised on the viscous scale, $p = p^*/(\mu U/R)$.

In a moving frame of reference, in which the bubble tip is fixed at the origin, the fluid motion is governed by the dimensionless, steady Navier–Stokes equations:

$$Re\ u_j \frac{\partial u_i}{\partial x_j} = -\frac{\partial p}{\partial x_i} + \frac{\partial}{\partial x_j}\left(\frac{\partial u_i}{\partial x_j} + \frac{\partial u_j}{\partial x_i}\right), \tag{2a}$$

and the continuity equation

$$\frac{\partial u_i}{\partial x_i} = 0, \tag{2b}$$

where $i, j = 1, 2, 3$ and the Einstein summation convention is used.

The boundary conditions at the free surface are the non-penetration condition

$$u_i n_i = 0, \tag{3}$$

and the dynamic (traction) boundary condition,

$$-p n_i + \left(\frac{\partial u_i}{\partial x_j} + \frac{\partial u_j}{\partial x_i}\right) n_j + \frac{1}{Ca}\kappa n_i = -p_b n_i. \tag{4}$$

Here $\boldsymbol{n}$ is the unit normal to the free surface (directed out of the fluid), $\kappa = \kappa^* R$ is the dimensionless curvature of the surface and $p_b = p^*_b/(\mu U/R)$ is the dimensionless internal bubble pressure.

The behaviour of the elastic tube is described by geometrically non-linear Kirchhoff–Love shell theory. We use Lagrangian co-ordinates, $\zeta^\alpha = \zeta^{*\alpha}/R$, $\alpha = 1, 2$ to parameterise the shell's midplane and the location of the undeformed midplane in the moving frame of reference is given by $\boldsymbol{r} = (\cos(\zeta^2), \sin(\zeta^2), \zeta^1)$. The deformation of the tube is specified by a displacement field, $\boldsymbol{v}$, and the position of the deformed midplane is thus $\boldsymbol{R} = \boldsymbol{r} + \boldsymbol{v}$.

In the present system, there are large bending deformations, but the strains remain small, and hence we use a linear constitutive equation (Hooke's law). The principle of virtual displacements, which describes the shell's deformation, is then

$$\int_0^{2\pi}\int_{-\infty}^{\infty} E^{\alpha\beta\gamma\delta}\left(\gamma_{\alpha\beta}\delta\gamma_{\gamma\delta} + \frac{1}{12}\left(\frac{h}{R}\right)^2 \kappa_{\alpha\beta}\delta\kappa_{\gamma\delta}\right)\,\mathrm{d}\zeta^1\mathrm{d}\zeta^2 =$$

$$\frac{1}{12}\left(\frac{h}{R}\right)^3 \frac{1}{1-\nu^2}\int_0^{2\pi}\int_{-\infty}^{\infty}\left(\frac{R}{h}\right)\boldsymbol{f}\cdot\delta\boldsymbol{R}\sqrt{A}\,\mathrm{d}\zeta^1\mathrm{d}\zeta^2, \tag{5}$$

where the Einstein summation convention is again used and the Greek indices take the values $\alpha = 1, 2$. $E^{\alpha\beta\gamma\delta}$ is the plane stress stiffness tensor, non-dimensionalised by Young's modulus; A is the determinant of the covariant metric tensor of the deformed midplane;

$\boldsymbol{f} = \boldsymbol{f}^*/K$ is the traction per unit area of the deformed midplane; finally, $\gamma_{\alpha\beta}$ and $\kappa_{\alpha\beta}$ are tensors quantifying the stretching and bending, respectively; see Hazel & Heil [10].

The interaction between the fluid and the elastic shell is imposed via two equations. Firstly, the no-slip boundary condition implies that the fluid velocity on the tube wall must be the same as the local wall velocity, and, in the moving frame of reference,

$$\boldsymbol{u} = \frac{\partial \boldsymbol{R}(\zeta^\alpha)}{\partial \zeta^1} \quad \text{on the tube walls.} \tag{6}$$

Secondly, the fluid exerts a traction on the shell, and the load terms in the solid equations (5) are given by

$$f_i = P^{(\text{ext})} N_i - \sigma Ca \left(p N_i - \left(\frac{\partial u_i}{\partial x_j} + \frac{\partial u_j}{\partial x_i} \right) N_j \right), \tag{7}$$

where $\boldsymbol{N}$ is the (inward) normal to the deformed shell midplane and $P^{(\text{ext})} = P^{(\text{ext})*}/K$ is the external pressure.

The weak form of the Navier–Stokes equations and the variational equations for the shell were discretised by finite elements. Within each fluid element, tri-quadratic basis functions were used to interpolate the fluid velocity components and the pressure was approximated by tri-linear functions [17]. Solid displacements and their derivatives were approximated using Hermite polynomials [18]. The position of the nodes in the fluid mesh were adjusted in response to changes in the free surface position and wall displacement via a generalisation of Kistler & Scriven's "Method of Spines" [19].

The computational domain was truncated at finite distances ahead and behind the bubble tip, where the axial gradients of the transverse wall displacements were set to zero. A long-wavelength approximation (lubrication theory) was used to determine the axial fluid velocities, subject to the constraint that the axial flowrate equals A_∞, and the results were applied as Dirichlet conditions at the ends of the domain. Traction-free boundary conditions were applied in the transverse directions and rigid body motions were suppressed by fixing the axial position of the end of the tube far behind the bubble tip. Finally, symmetry was imposed in the planes $x_1 = 0$ and $x_2 = 0$, and the computational domain was restricted to positive values of the transverse coordinates, $x_1 \geq 0$, $x_2 \geq 0$ and $\zeta^2 \in [0, \pi/2]$.

The system of non-linear algebraic equations was solved using a Newton–Raphson method and a frontal scheme [20] was used to assemble and solve the resulting linear systems. For a typical initial guess, the residuals are of $\mathcal{O}(1)$ and the Newton iteration was deemed to have converged when the absolute value of the largest residual was less than 10^{-8}. The results at $Re = 0$ from Hazel & Heil's study [10] were used as initial conditions and then Re was increased incrementally. Further details of the formulation and validation of the solvers may be found in references [10, 21]. The spatial convergence of the results was assessed by repeating selected studies with higher spatial resolution; see Fig. 2.

3 Numerical Results

Throughout this paper we used a Poisson's ratio of $\nu = 0.49$ to reflect the near-incompressibility of lung tissue, and set the wall thickness to $h/R = 1/20$, close to the upper limit of applicability of thin-shell theory. The external (pleural) pressure was set to zero, $P^{(\text{ext})} = 0$, and hence the fluid pressure is negative in regions where the tube is compressed. The default value for the tube's cross-sectional area far ahead of the air finger is $A_\infty = 0.373$, which corresponds to maximum inward radial displacement of 80% of the tube's undeformed radius and unless otherwise stated we used a non-dimensional surface tension of $\sigma = 1$.

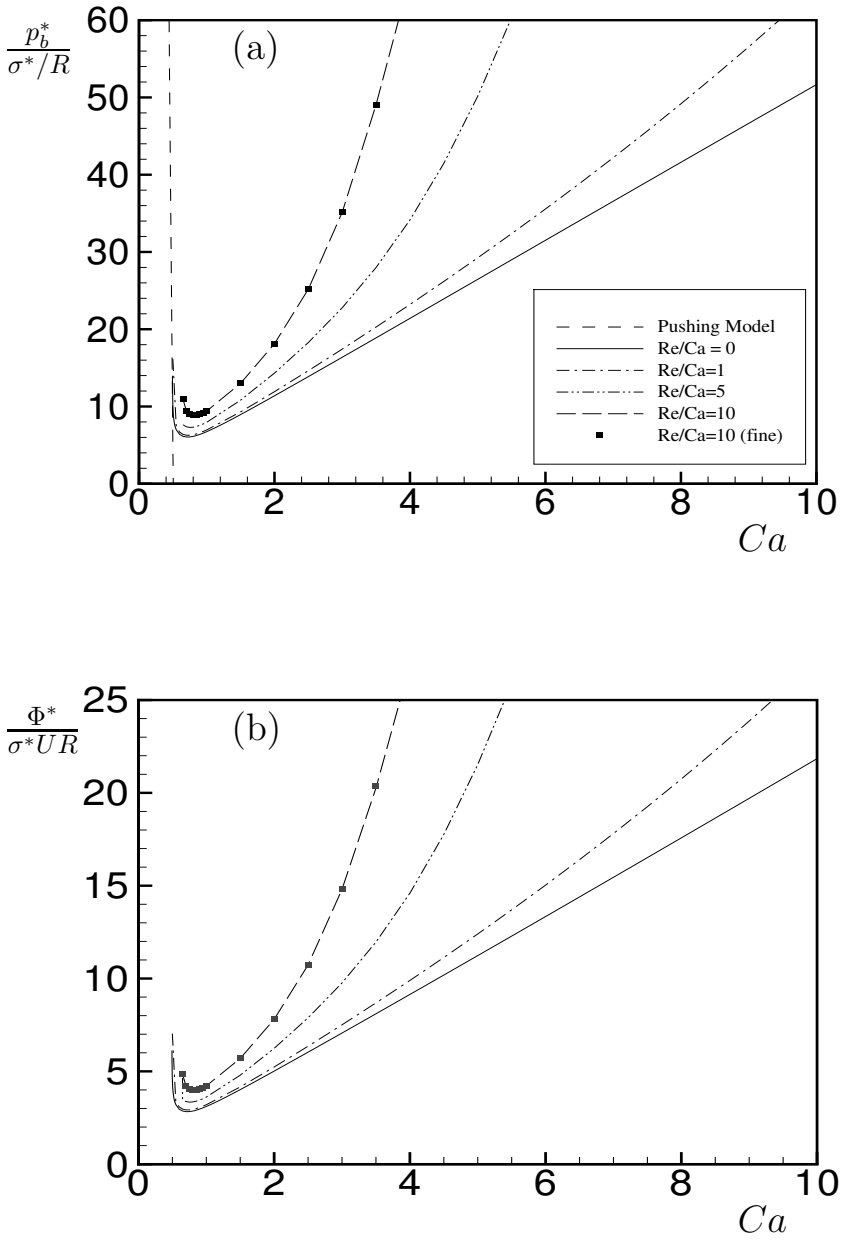

Figure 2: (a) Bubble pressure vs. capillary number for $A_\infty = 0.373$, $\sigma = 1.0$ and $Re/Ca = 0$, 1, 5, 10. The markers show the results for $Re/Ca = 10$ on a refined mesh (83,000 degrees of freedom). They differ by less than 0.5% from the results at the standard resolution (43,000 degrees of freedom). The dashed line is the result from Hazel & Heil's [10] asymptotic model for the 'pushing' branch at zero Reynolds number. (b) The total viscous dissipation, Φ, vs. capillary number for the same parameter values as in (a).

3.1 Effects of fluid inertia

In any experimental setup, consisting of a given working fluid and a given elastic tube, σ will be constant, as will the ratio $Re/Ca = \rho R \sigma^*/\mu^2$, which depends only upon material

parameters and not the bubble speed U. We shall, therefore, assess the effects of fluid inertia on the system by examining curves of bubble pressure versus propagation speed for fixed values of the ratio Re/Ca, rather than for fixed values of Re. These curves correspond to experiments in which the speed of the the air finger is increased, for example, by increasing the flowrate, but all other physical parameters remain constant. Fig. 2(a) shows such curves for $\sigma = 1$, $A_\infty = 0.373$ and for $Re/Ca = 0$, 1, 5 and 10. Representative tube shapes and pressure distributions at a capillary number of $Ca = 4$ are shown in Fig. 3 for $Re/Ca = 0$ and $Re/Ca = 10$.

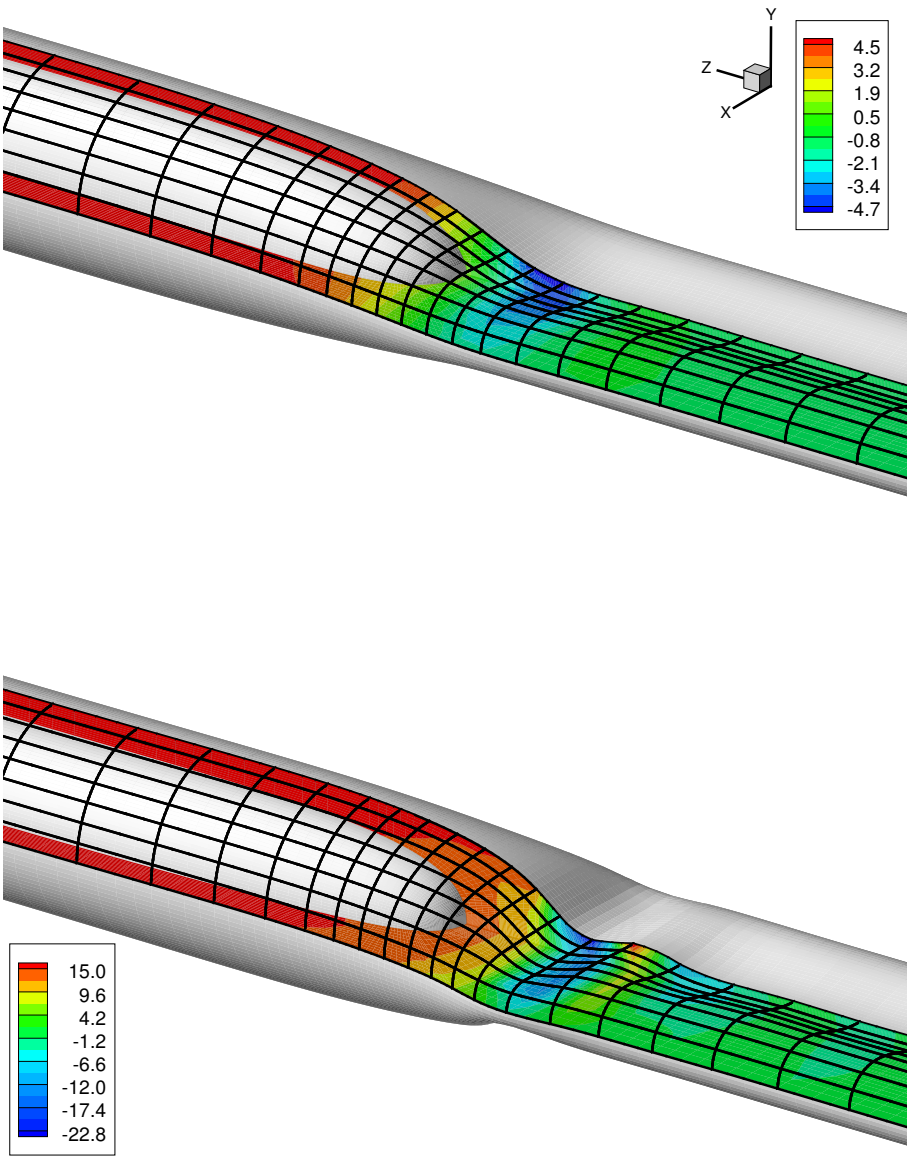

Figure 3: Interface and wall shapes for $Ca = 4$ and $Re/Ca = 0$ (top), 10 (bottom). Contours of pressure in the planes $x_1 = 0$ and $x_2 = 0$ are also shown.

The results indicate that even relatively weak fluid inertia has a very strong effect on the system's behaviour. In particular, Fig. 2(a) shows that, compared to the case of zero

Reynolds number, much larger bubble pressures are required to drive the air finger at a given capillary number. Inertial effects become more pronounced as Ca increases, owing to the corresponding increase in $Re = \text{Constant} \times Ca$. Conversely, at small values of Ca, and hence Re, inertial effects become negligible and Hazel & Heil's 'pushing' model [10] provides a good approximation for the system's behaviour at all values of Re/Ca. These results are qualitatively similar to those of Heil's [16] two-dimensional model, which also predicted that increasing Re/Ca leads to an increase in the bubble pressure at a fixed Ca. The two- and three-dimensional systems are, of course, very different and it is not possible to make a direct comparison between the two sets of results.

Fig. 3 demonstrates that the presence of fluid inertia also leads to significant changes in the wall and interface shapes. At zero Reynolds number, a region of low pressure develops ahead of the finger tip, leading to a local minimum in the tube's cross sectional area. Similar wall shapes have been observed in two-dimensional models, in which the resulting 'neck' ahead of the finger tip can be identified as the first minimum of a damped oscillatory eigenfunction for the wall displacement field (see, e.g., [9, 22]). At finite Reynolds number, the amplitude of the oscillatory wall displacement field increases and the subsequent maxima and minima of the cross sectional area (and the associated variations in fluid pressure) become clearly noticeable. This behaviour is consistent with the Bernoulli effect: in the more strongly collapsed cross sections, the fluid velocity increases and, in the presence of fluid inertia, the local fluid pressure is reduced. The reduced fluid pressure causes an increase in the local wall compression, increasing the amplitude of the oscillatory wall displacement field. In addition to the changes in the wall shape, an increase in Reynolds number causes the air-liquid interface to move further away from the tube wall (see also Fig. 5, below).

The increase in the amplitude of the oscillatory wall displacement field and the movement of the air-liquid interface both lead to an increase in the size of the region in which the fluid velocity is spatially non-uniform (in the moving frame of reference the fluid has a uniform velocity far ahead and far behind the bubble tip). Hence the changes in the shape of the fluid domain induced by fluid inertia lead to an increase in the viscous dissipation in the system; see Fig 2(b). The dimensionless total viscous dissipation, Φ, is defined by

$$\Phi = \frac{\Phi^*}{\sigma^* U R} = \frac{1}{2}\, Ca \iiint \left(\frac{\partial u_i}{\partial x_j} + \frac{\partial u_j}{\partial x_i} \right)^2 dV; \tag{8}$$

and the non-dimensionalisation is consistent with the capillary pressure scale used in Fig. 2(a). If the viscous dissipation increases, then the total energy input into the system per unit time must also increase, which requires an increase in the driving bubble pressure. Note that increasing the bubble pressure also causes an increase in tube's cross-sectional area far behind the bubble tip, which can release stored elastic energy if the tube is partially collapsed in this region. Conversely, if the tube is inflated behind the bubble tip, part of the additional energy provided by increasing the bubble pressure is converted into elastic energy stored in the strained tube. In either case, the net effect of an increase in viscous dissipation is to cause an increase in the bubble pressure, p_b, required to drive the air finger at a given speed.

The changes to the wall shape caused by the Bernoulli effect are likely to be responsible for the rapid increase in bubble pressure with the capillary number. An increase in bubble speed amplifies the Bernoulli effect and thus causes an even stronger compression of the tube wall in the region ahead of the finger tip. Ultimately, the strong feedback between fluid velocity, fluid pressure and wall shape can lead to 'flow limitation', where the velocity cannot exceed a critical value: a phenomenon well-known in collapsible tube theory [23]. The onset of 'flow limitation' may be observed in Fig. 2 where the slope of the $Re/Ca = 10$ curve increases very rapidly with Ca.

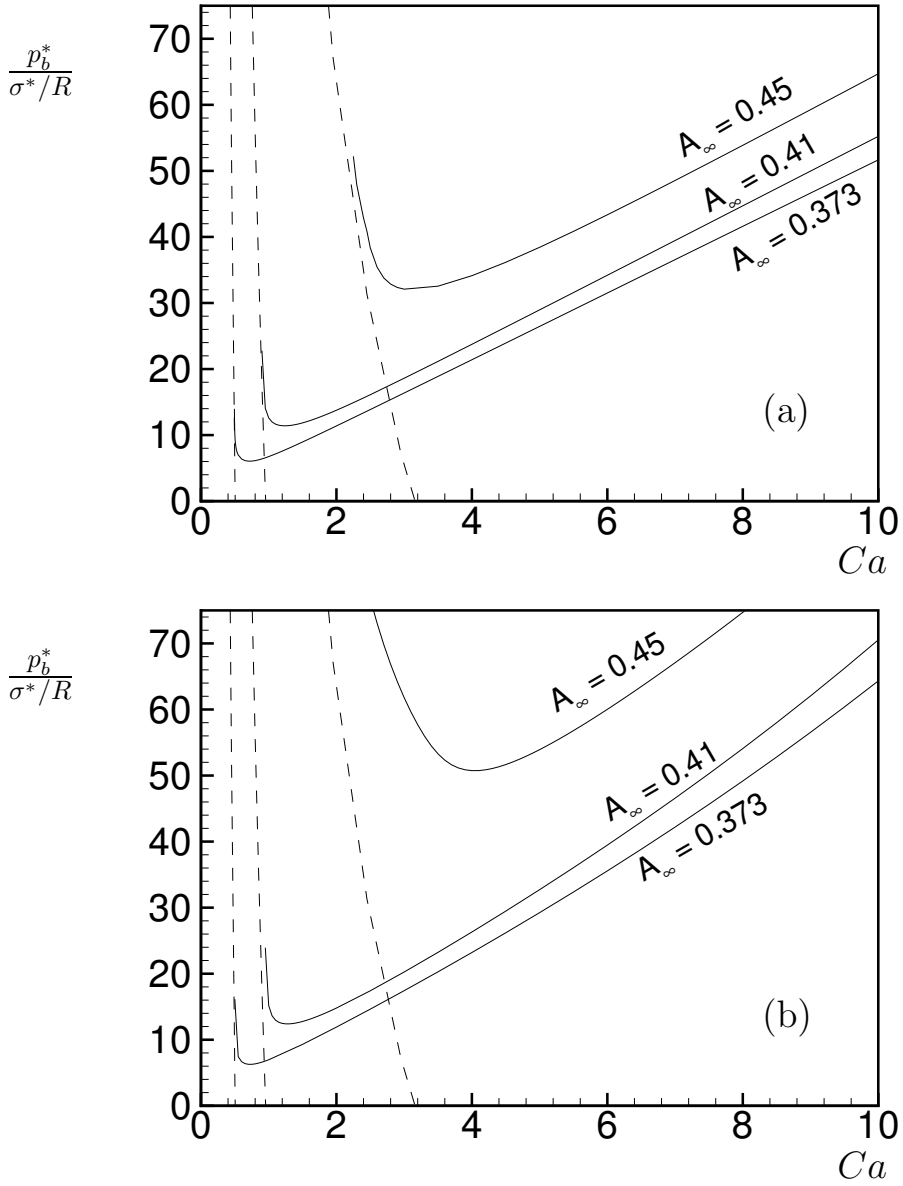

Figure 4: Bubble pressure vs. dimensionless propagation speed for $A_\infty = 0.373$, 0.41, 0.45 for $\sigma = 1$ and (a) $Re = 0$ and (b) $Re/Ca = 1$.

3.2 Effect of the initial degree of collapse, A_∞

Hazel & Heil's study [10] showed that the tube's degree of collapse far ahead of the bubble tip, characterised by A_∞, is an important parameter in the problem. They found that, at zero Reynolds number, "it is easier to reopen a more strongly buckled tube"; see Fig. 4(a). The explanation for this behaviour was again based on an examination of the viscous dissipation in the system. If the tube's cross sectional area far ahead of the finger is increased then a larger volume of fluid needs to be redistributed per unit time. Consequently, a larger bubble pressure is required to drive the air finger at a given Ca.

Fig. 4(b) indicates that at finite Reynolds number, the same trends are observed and further that the influence of fluid inertia is more pronounced at larger values of A_∞. For example, an increase of Re/Ca from 0 to 1 causes an increase of ≈ 0.2 in $p_{\min}$ for $A_\infty = 0.373$, but the increase is ≈ 20 when $A_\infty = 0.45$.

To explain this behaviour, Fig. 5 shows the shapes of the tube wall and the air-liquid interface in the axial plane $x_1 = 0$ at $Ca = 6$ for $A_\infty = 0.373$, 0.41, 0.45 at $Re/Ca = 0$ (dashed) and 1 (solid). The figure shows that for a given increase in Re/Ca, the changes in the wall shape are more dramatic at higher A_∞. In particular, for $A_\infty = 0.45$ the increase in the distance between the air-liquid interface and the tube wall is more pronounced than for the more strongly collapsed tubes. These changes in wall shape are consistent with the greater relative changes in bubble pressure with Re/Ca for less strongly collapsed tubes, although the precise details of the mechanism responsible for this behaviour are unclear. Nevertheless, the net effect of fluid inertia is to cause an increase in the total viscous dissipation, which causes a corresponding increase in the bubble pressure at a given Ca.

3.3 The non-axisymmetry of the deposited film

In the transition region between the collapsed and reopened parts of the tube, both the tube wall and the air-liquid interface are strongly non-axisymmetric; see Fig. 3. In the region behind the finger tip the non-axisymmetry of the air-liquid interface generates surface tension forces that drive the fluid towards a configuration in which the air-liquid interface is axisymmetric. Furthermore, in the three cases shown in Fig. 5 the bubble pressure, p_b, is so large that the wall is subject to a positive transmural pressure so that the tube is inflated. Hence, at large distances behind the finger tip, both the tube wall and the air-liquid interface approach axisymmetric shapes. Hazel & Heil's study of the propagation of air fingers into rigid-walled, fluid-filled tubes of non-circular cross-section [21] demonstrated that, at large capillary numbers, the evolution towards an axisymmetric air-liquid interface occurs over very large axial distances. The plots of the wall and air-liquid interface shapes in the cross-sectional planes $x_3 = 4$, shown in Fig. 6, show the same phenomenon in the present problem. In all cases, the air-liquid interface remains strongly non-axisymmetric for considerable distances behind the bubble tip. The non-axisymmetry persists further at smaller values of A_∞ because a reduction in A_∞ reduces the thickness of the film that is deposited on the tube wall. Thinner films offer a larger viscous resistance to the surface-tension-driven azimuthal flows that redistribute the fluid in the liquid lining towards its axisymmetric equilibrium configuration. As a result, the azimuthal redistribution of fluid occurs over larger axial distances. Fig. 6 shows that an increase in Re/Ca reduces the non-axisymmetry of the air-liquid interface; this effect is enhanced at larger values of A_∞. For instance, for $A_\infty = 0.373$, an increase in Re/Ca from 0 to 1 reduces the ratio of the maximum and minimum radii of the air-liquid interface in the cross-sectional plane $x_3 = 4$ from $r_{max}/r_{min} = 1.31$ to 1.29; at $A_\infty = 0.45$ the same increase in Re/Ca changes the ratio from 1.18 to 1.07.

4 Discussion

We have shown that fluid inertia can have a surprisingly strong effect on the pressure required to reopen a collapsed, fluid-filled airway by a steadily propagating air finger. The results obtained from our 3D computations are qualitatively similar to those reported in reference [16] where a simpler 2D model problem was considered. In both systems, fluid inertia primarily causes changes to the wall and interface shapes that increase the total viscous dissipation and, therefore, increase the bubble pressure, p_b, required to drive the air finger at a given speed. Hence, models that neglect fluid inertia will underpredict the value of p_b.

The relative importance of fluid inertia is governed by the ratio of Reynolds and capillary numbers, $Re/Ca = \rho R\sigma/\mu^2$, a material parameter. The values of Re/Ca considered in the present study are appropriate for typical "benchtop" airway reopening experiments (see reference [16] for a compilation of typical parameter values). If we choose parameter values that are representative of the conditions in the small airways

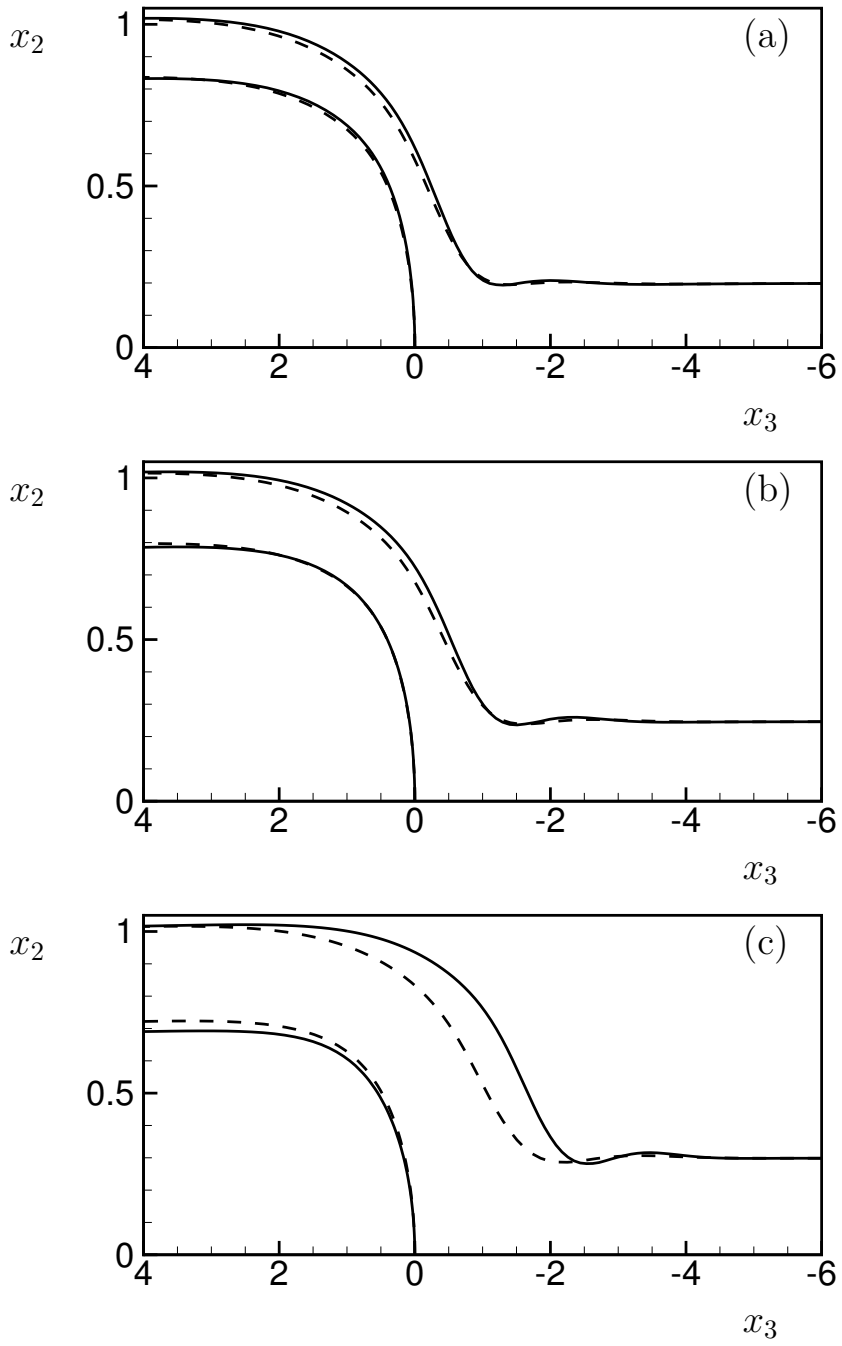

Figure 5: Axial slices in the plane $x_1 = 0$, showing the airway wall and the air-liquid interface for $Re/Ca = 1$ (solid lines) and $Re/Ca = 0$ (dashed lines). (a) $A_\infty = 0.373$; (b) $A_\infty = 0.41$; (c) $A_\infty = 0.45$. In all three cases $Ca = 6$ and $\sigma = 1$.

of the lung where the properties of the lining fluid are similar to those of water ($R = 2.5 \times 10^{-4}$m, $\rho = 1000$ kg/m^3, $\gamma = 0.02$ kg/sec^2, $\mu = 10^{-3}$kg/(m sec); see reference [4]),

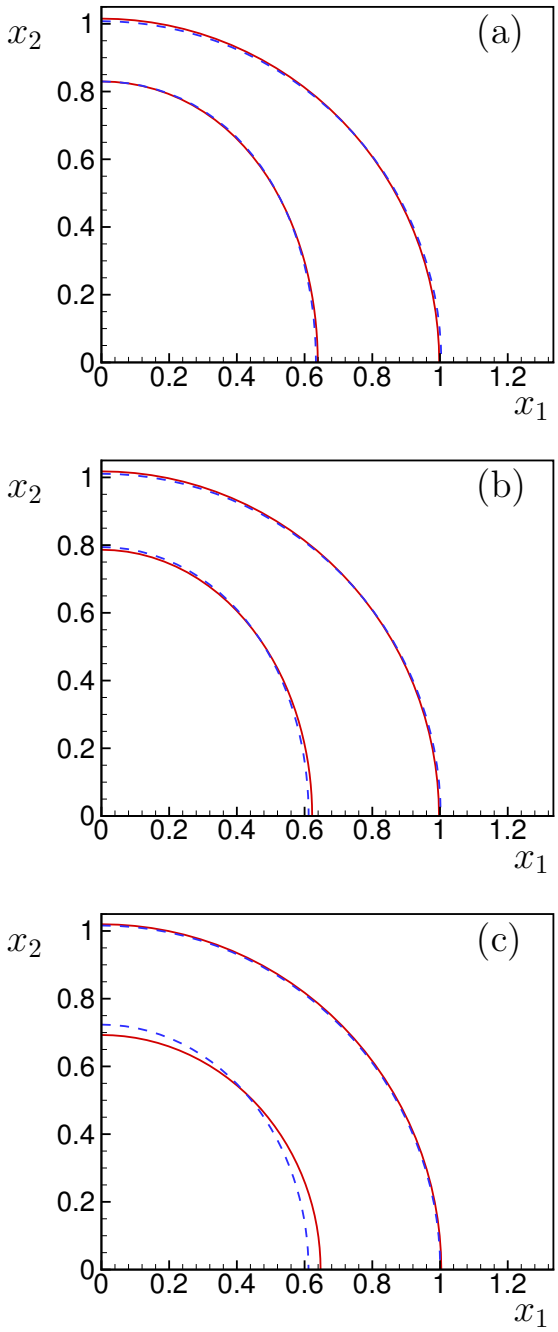

Figure 6: Transverse cross-sections in the plane $x_3 = 4$ for the same parameter values as in Fig. 5. Solid lines: $Re/Ca = 1$; dashed lines $Re/Ca = 0$. The outer lines represent the airway wall, the inner lines the air-liquid interface.

we obtain a much larger value of $Re/Ca = 5000$. This suggests that inertial effects are likely to play an important role during pulmonary airway reopening.

Although our 3D model presents a considerable improvement over previous 2D models, it is still an extreme simplification of the conditions in the pulmonary airways. For instance, our model ignores the complicated multi-layer structure of the airway wall and the external tethering provided by the parenchyma. In addition, we assumed a constant value for the surface tension, σ^*, whereas the spatially non-uniform distribution of pulmonary surfactant in the lung leads to spatial variations in surface tension along the air-liquid interface. Most of these effects could easily be incorporated into our model — at the cost of a significant increase in the number of control parameters. The effect of surfactant on airway reopening has so far only been analysed in the context of 2D model problems (e.g. [12, 13]). We expect that the pronounced non-axisymmetry of the air-liquid interface and the resulting, surface-tension-driven azimuthal flows in the region behind the finger tip, documented in Fig. 6, may have a strong effect on (and be strongly affected by) the surfactant transport.

We believe that the most significant shortcoming of the present model is the assumption that the air finger propagates steadily. If airway reopening is driven by a prescribed pressure and if the "pushing branch" is indeed unstable under these conditions (as suggested by Halpern *et al.*'s analysis of the corresponding 2D system, [11]), then steady reopening would require capillary numbers of at least $Ca \approx 0.5$ (see Figs. 2 and 4). Based on the above parameter estimates, this capillary number corresponds to a dimensional propagation speed of $U = 10$ m/sec, suggesting that the reopening process is likely to be dominated by transient, unsteady effects as the air finger proceeds rapidly through the multiple bifurcations of the pulmonary tree. Alternatively, if the process is intrinsically unsteady, reopening could occur at much slower speeds with bubble pressures below the minimum pressure, p_{min}, required for the steady reopening.

Acknowledgements

Financial support from the EPSRC is gratefully acknowledged. The authors wish to acknowledge many helpful and enjoyable discussions with Dr. Anne Juel and Alexandra Heap. The HSL library routine MA42 : a frontal solver for sparse, unsymmetric systems and the cfortran.h header file were used in the development of the numerical code in this work.

References

[1] N. B. Pride and P. T. Macklem. Lung mechanics in disease. In *Handbook of physiology. Section 3: The Respiratory System,*, pages Vol III, Part 2, 659–692. American Physiological Society, 1986.

[2] J. M. B. Hughes, D. Y. Rosenzweig, and P. B. Kivitz. Site of airway closure in excised dog lungs: histologic demonstration. *Journal of Applied Physiology*, 29:340–344, 1970.

[3] P. T. Macklem, D. F. Proctor, and J. C. Hogg. The stability of the peripheral airways. *Respiratory Physiology*, 8:191–203, 1970.

[4] D. Halpern and J. B. Grotberg. Fluid-elastic instabilities of liquid-lined flexible tubes. *Journal of Fluid Mechanics*, 244:615–632, 1992.

[5] M. Heil and J. P. White. Airway closure: surface-tension-driven non-axisymmetric instabilities of liquid-lined elastic rings. *Journal of Fluid Mechanics*, 462:79–109, 2002.

[6] J. P. White and M. Heil. Three-dimensional instabilities of liquid-lined elastic tubes: a thin-film, fluid-structure interaction model. *Physics of Fluids*, 17:031506, 2005.

[7] A. L. Hazel and M. Heil. Surface-tension-induced buckling of liquid-lined elastic tubes: a model for pulmonary airway closure. *Proceedings of the Royal Society A*, 461:1847–1868, 2005.

[8] D. P. III Gaver, R. W. Samsel, and J. Solway. Effects of surface tension and viscosity on airway reopening. *Journal of Applied Physiology*, 369:74–85, 1990.

[9] D. P. III Gaver, D. Halpern, O. E. Jensen, and J. B. Grotberg. The steady motion of a semi-infinite bubble through a flexible walled channel. *Journal of Fluid Mechanics*, 319:25–56, 1996.

[10] A. L. Hazel and M. Heil. Three-dimensional airway reopening: The steady propagation of a semi-infinite bubble into a buckled elastic tube. *Journal of Fluid Mechanics*, 478:47–70, 2003.

[11] D. Halpern, S. Naire, O. E. Jensen, and D. P. Gaver. Unsteady bubble propagation in a flexible-walled channel: predictions of a viscous stick-slip instability. *Journal of Fluid Mechanics*, 528:53–86, 2005.

[12] D. Y. K. Yap and D. P. III Gaver. The influence of surfactant on two-phase flow in a flexible-walled channel under bulk equilibrium conditions. *Physics of Fluids*, 10:1846–1863, 1998.

[13] S. Naire and O. E. Jensen. Epithelial cell deformation during surfactant-mediated airway reopening: a theoretical model. *Journal of Applied Physiology*, 99:458–471, 2005.

[14] M. Horsburgh. *Bubble propagation in flexible and permeable channels*. PhD thesis, Cambridge University, Cambridge, 2000.

[15] O.E. Jensen, M.K. Horsburgh, D. Halpern, and D.P. III Gaver. The steady propagation of a bubble in a flexible-walled channel: asymptotic and computational models. *Physics of Fluids*, 14:443–457, 2002.

[16] M. Heil. Finite Reynolds number effects in the propagation of an air finger into a liquid-filled flexible-walled tube. *Journal of Fluid Mechanics*, 424:21–44, 2000.

[17] C. Taylor and P. Hood. A numerical solution of the Navier-Stokes equations using the finite element technique. *Computers and Fluids*, 1:73–100, 1973.

[18] F. K. Bogner, R. L. Fox, and L. A. Schmit. A cylindrical shell discrete element. *AIAA Journal*, 5:745–750, 1967.

[19] S. F. Kistler and L. E. Scriven. Coating flows. In J. R. A. Pearson and S. M. Richardson, editors, *Computational analysis of polymer processing.*, pages 243–299. Applied Science Publishers, London, 1983.

[20] I. S. Duff and J. A. Scott. The design of a new frontal code for solving sparse, unsymmetric linear systems. *ACM Transactions on Mathematical Software*, 22:30–45, 1996.

[21] A. L. Hazel and M. Heil. The steady propagation of a semi-infinite bubble into a tube of elliptical or rectangular cross-section. *Journal of Fluid Mechanics*, 479:91–114, 2002.

[22] M. Heil. The Bretherton problem in elastic-walled channels: Finite Reynolds number effects. In Y.D. Shikmurzaev, editor, *IUTAM Symposium on Free Surface Flows*, pages 113–120, Dordrecht, Netherlands, 2001. Kluwer.

[23] M. Heil and O. E. Jensen. Flows in deformable tubes and channels – theoretical models and biological applications. In T. J. Pedley and P. W. Carpenter, editors, *Flow in Collapsible Tubes and Past Other Highly Compliant Boundaries*, pages 15–50, Dordrecht, Netherlands, 2003. Kluwer.